Andreev bound states in iron pnictide superconductors

Wen-Min Huang[1] and Hsiu-Hau Lin[1,2]
[1]*Department of Physics, National Tsing Hua University, Hsinchu 30013, Taiwan*
[2]*Physics Division, National Center for Theoretical Sciences, Hsinchu 30013, Taiwan*
(Received 1 December 2009; published 12 February 2010)

Andreev bound states have been proposed as an experimental probe to detect the pairing symmetry in iron pnictide superconductors. However, previous theoretical studies show that the local density of states below the superconducting gap is small, making the detection rather challenging in experiments. We revisit this important issue from the Bogoliubov-de Gennes Hamiltonian and carefully include both the lattice effects and the boundary potentials. It is rather surprising that significant spectral weights in the midgap regime emerge, leading to easy detection for the Andreev bound states in realistic experiments. Furthermore, pronounced peaks appear in the momentum-resolved local density of states and enhance quasiparticle interferences at specific momenta. We analyze the locations of these magic spots from quasiparticle interferences and propose a direct experimental verification by the Fourier-transformed scanning tunneling spectroscopy.

DOI: 10.1103/PhysRevB.81.052504 PACS number(s): 74.45.+c, 74.78.−w, 74.20.−z

Recent discovery of iron pnictide superconductors[1–4] reignites intense explorations on the unconventional superconductivity.[5,6] As the first step to reveal the underlying pairing mechanism, it is of crucial importance to understand the pairing symmetry in iron pnictides. The signature of nodes in the superconducting gap is suggested by the recent nuclear-magnetic-resonance experiments[7,8] and also the measurements for the penetration depth[9–12] and the specific heat.[13] On the other hand, some other experiments[14–17] show the opposite without any hint for the nodes. In particular, the angular-resolved photoemission spectroscopy[18–21] clearly demonstrates the full gap at all points on the Fermi surface. Therefore, the pairing symmetry remains an important issue with controversy at the point of writing.

Band-structure calculations[22,23] show that the low-energy excitations mainly arise from the two-dimensional FeAs layers with two disconnected holelike and electronlike Fermi surfaces. Nesting between the hole and electron pockets causes the magnetic ordering before the superconductivity sets in, hinting that the spin fluctuations may play a significant role in pairing mechanism.[14,21,24] Renormalization-group analysis[25–27] suggests that the pairing symmetry is the extended s wave (or the $s_{\pm}$ wave)—full gaps on both hole and electron pockets but with opposite signs in the gap functions. The unconventional $s_{\pm}$-wave pairing stimulates intense studies[28–33] and its role in the pairing mechanism and the potential connection to the magnetic instabilities are under investigations.

Andreev bound states (ABSs) (Ref. 33) can serve as an indirect probe for the $s_{\pm}$-wave paring. In contrast to the d-wave pairing symmetry in cuprates,[34] ABS in iron pnictides appears at finite energy with dispersion depending on the microscopic details. Current theoretical studies[33] find that the local density of states is small in the midgap regime and posts a challenging task for experimental detection. Here, we revisit this important problem with care, including both the lattice effects and also the boundary potential from the work function near the sample edges. In contrast to the previous results, we find large spectral weights in the midgap regime and significant peaks in the momentum-resolved local density of states. In addition, we also predict the locations of the magic spots arisen from quasiparticle interferences, which can be verified by the Fourier-transformed scanning tunneling spectroscopy (FT-STS).[35,36]

We use the two-orbital Bogoliubov-de Gennes (BdG) Hamiltonian to model the iron pnictide on the square lattice,

$$H_{BdG}=\sum_{a,b}\sum_{\boldsymbol{r},\boldsymbol{r}';\sigma}[t_{ab}(\boldsymbol{r},\boldsymbol{r}')-\mu\delta_{a,b}\delta_{\boldsymbol{r},\boldsymbol{r}'}]c^{\dagger}_{a\sigma}(\boldsymbol{r})c_{b\sigma}(\boldsymbol{r}')+\sum_{a,b}\sum_{\boldsymbol{r},\boldsymbol{r}'}[\Delta^{*}_{ab}(\boldsymbol{r},\boldsymbol{r}')c_{a\uparrow}(\boldsymbol{r})c_{b\downarrow}(\boldsymbol{r}')+\text{H.c.}],\quad(1)$$

where σ labels the spins and $a,b=X,Y$ denote the d_{XZ} and d_{YZ} orbitals, respectively. The nonvanishing hopping amplitudes t_{ab} on the square lattice include the intraorbital hopping $t_{XX}(x\pm1,y)=t_{YY}(x,y\pm1)=-t_1$, $t_{XX}(x,y\pm1)=t_{YY}(x\pm1,y)=-t_2$, $t_{XX/YY}(x\pm1,y\pm1)=t_{XX/YY}(x\mp1,y\pm1)=-t_3$ and the interorbital hopping $t_{XY}(x\pm1,y\pm1)=-t_{XY}(x\mp1,y\pm1)=t_4$. The lattice constant is set to unity $a=1$ throughout this Brief Report. With appropriate parameters, it was shown that the two-band model captures the essential features of the realistic band structure.[37,38] The Fermi surface contains two electron pockets at the X and Y points and two hole pockets at the Γ and M points in the Brillouin zone as shown in Fig. 1. We consider the gap function with the $s_{\pm}$-wave symmetry, described by the intraorbital pairing $\Delta_{XX/YY}(x\pm1,y\pm1)=\Delta_{XX/YY}(x\mp1,y\pm1)=\Delta_0$ on the square lattice shown in Fig. 1. Although the gap function does not change sign on the square lattice, it takes the form $\Delta(\boldsymbol{k})=4\Delta_0\cos k_x\cos k_y$ in the momentum space and thus carries opposite signs in the electron and the hole pockets as shown in Fig. 1.

The translational invariance along the y direction makes the momentum k_y a good quantum number. The open boundary ruins the translation invariance in the x direction but the solution can be constructed from the generalized Bloch state,[39,40] $\Phi_z(x)=\Phi z^x$, where z is the (complex) eigenvalue of the displacement operator, $D\Phi_z(x)=z\Phi_z(x)$. The BdG Hamiltonian is block diagonal for different k_y momenta and the eigenvalue problem is greatly simplified to $(H_z-\epsilon\mathbf{1})\Phi=0$ or in the matrix form explicitly,

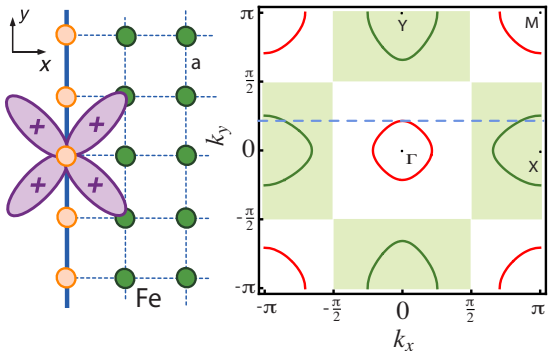

FIG. 1. (Color online) A semi-infinite square lattice for iron pnictide with a flat edge. The surface potential V_0 locates along the boundary sites colored in orange. The Fermi surface of the two-band model with tight-binding parameters $t_1=-1$, $t_2=1.3$, $t_3=t_4=0.85$, and $\mu=1.55$ is shown. The pairing potential on the lattice and in the momentum space is shown here and the shaded area in the Brillouin zone denotes the sign change in the gap function. The blue dashed line stands for the transverse momentum where the hole pocket near the Γ point vanishes.

$$\begin{pmatrix} T_{11}-\epsilon & T_{12} & \Delta_{11} & 0 \\ T_{21} & T_{22}-\epsilon & 0 & \Delta_{22} \\ \Delta_{11} & 0 & -T_{11}-\epsilon & -T_{12} \\ 0 & \Delta_{22} & -T_{12} & -T_{22}-\epsilon \end{pmatrix} \begin{pmatrix} \phi_{1\uparrow} \\ \phi_{2\uparrow} \\ \phi_{1\downarrow} \\ \phi_{2\downarrow} \end{pmatrix} = 0, \tag{2}$$

where $T_{11}=t_{11}/z-(\mu_1+\mu)+t_{11}z$, $T_{22}=t_{22}/z-(\mu_2+\mu)+t_{22}z$, $T_{12}=-it_{12}/z+it_{12}z$, and $\Delta_{11}=\Delta_{22}=\Delta_1/z+\Delta_1 z$. The effective hopping amplitudes and the gap functions are $t_{11}=-t_1-2t_3\cos k_y$, $\mu_1=-2t_2\cos k_y$, $t_{22}=-t_2-2t_3\cos k_y$, $\mu_2=-2t_1\cos k_y$, $t_{12}=2t_4\sin k_y$, and $\Delta_1=2\Delta_0\cos k_y$. For given k_y and ϵ, one can find eight solutions for z with corresponding eigenvectors Φ. Unit modulus $|z|=1$ solutions are the usual plane waves, and $|z|<1$ corresponds to the evanescent modes near the open boundary. Note that z and $1/z$ solutions come in pairs and thus at most four $|z|<1$ evanescent modes are expected.

Construct the general solution $\Psi(x)=\Sigma_{\gamma=1}^{4}a_\gamma\Phi_\gamma(x)$ to account for the boundary conditions. Due to the work function near the sample edge, we introduce V_0 to incorporate the rise in the potential energy near the open boundary. After some algebra, the boundary conditions can be cast into the matrix form,

$$\boldsymbol{B}_c\Psi(-1)+\boldsymbol{V}\Psi(0)=0, \tag{3}$$

with

$$\boldsymbol{B}_c=\begin{pmatrix} t_{11} & -it_{12} & \Delta_1 & 0 \\ -it_{12} & t_{22} & 0 & \Delta_1 \\ \Delta_1 & 0 & -t_{11} & it_{12} \\ 0 & \Delta_1 & it_{12} & -t_{22} \end{pmatrix}, \quad \boldsymbol{V}=V_0\begin{pmatrix} \mathbf{1} & \mathbf{0} \\ \mathbf{0} & -\mathbf{1} \end{pmatrix}, \tag{4}$$

where $\mathbf{1}$ is the 2×2 identity matrix. Substituting the wave function $\Psi(x)$ into Eq. (3), the boundary conditions simplifies, $(\boldsymbol{B}_c\boldsymbol{N}'+\boldsymbol{V}\boldsymbol{N})A=0$, where $A=(a_1,a_2,a_3,a_4)$, $\boldsymbol{N}'=(\frac{1}{z_1}\Phi_1,\frac{1}{z_2}\Phi_2,\frac{1}{z_3}\Phi_3,\frac{1}{z_4}\Phi_4)$, and $\boldsymbol{N}=(\Phi_1,\Phi_2,\Phi_3,\Phi_4)$. The determinant must vanish, $\det[\boldsymbol{B}_c\boldsymbol{N}'+\boldsymbol{V}\boldsymbol{N}]=0$, to allow nontrivial solutions.

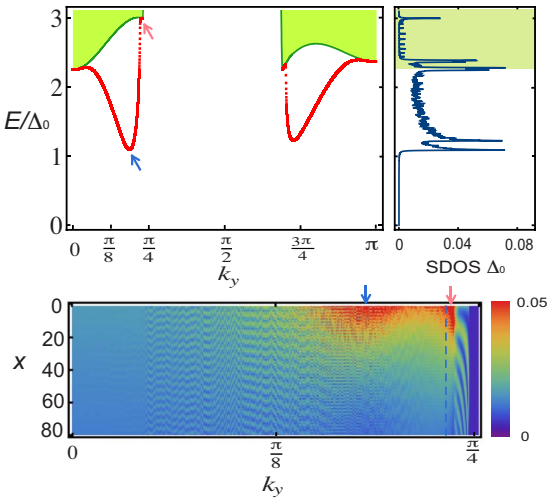

FIG. 2. (Color online) Dispersion of ABS with $\Delta_0=0.004$ (corresponding to the realistic values of ~15 meV for the superconducting gap) is shown in the upper-left panel. The surface potential $V_0/|t_1|=0.16$ is chosen here. The green shaded areas denote the continuum from the bulk states. The surface density of states is plotted in the upper-right panel and the momentum-solved probability density is shown in the lower panel. The blue dashed line stands for the transverse momentum where the hole pocket vanishes as in Fig. 1.

Solving the generalized Bloch state at each momentum k_y, the full dispersion for the ABS is obtained. Since it is symmetric around $k_y=0$, only the portion between $k_y=0$ and $k_y=\pi$ is shown in Fig. 2. The continuum for the quasiparticles in the bulk (shaded green area) contains two sectors: the left part (with $0\leq k_y\lesssim\pi/4$) corresponds to the Fermi surface near the Γ and X points in the Brillouin zone, and the right part are for the regimes close to the Y and M points. Since we do not linearize the energy spectrum near the Fermi surface, our approach eliminates all artifacts in the vicinity where the ABS merges into the continuum smoothly. The most important feature of the dispersion are the dips located at the transverse momenta $q_1\simeq\pm0.19\pi$ (near the Γ/X points) and $q_2\simeq\pm0.72\pi$ (near the Y/M points). These dip structures give rise to large spectral weights inside the midgap regime and also enhance quasiparticle interferences at specific momenta.

Let us first focus on the surface density of states (SDOS), i.e., the local density of states near the boundary. It can be computed numerically, $D_s(E)=(1/L_y)\Sigma_{k_y}|\Psi(x=0,k_y)|^2\delta[E-\epsilon(k_y)]$, with the peak structure shown in Fig. 2. The peaks inside the continuum hybridize with the plane-wave states and are unlikely to remain sharp in realistic situations. On the other hand, the evanescent modes in the midgap regime are protected and remain robust. In sharp contrast to the previous studies, we find that the spectral weights in the midgap regime are significant. Two pronounced peaks, arisen from the dips in the dispersion, can be detected in tunneling junc-

tions or related experimental setups. Compared with previous studies, two ingredients included in our calculations explain the major differences: the lattice effects for the band structure and the boundary potential arisen from the work function near the sample edge. The large spectral weights render the experimental detection for the ABS easier and may serve as an indirect probe for the pairing symmetry.

The probability density $|\Psi(x,k_y)|^2$ with momentum resolution is shown in the bottom part of Fig. 2. For clarity, we only show the momentum range $0 \leq k_y \leq \pi/4$ near the Γ/X points. In the vicinity of $k_y=\pi/4$, there is no ABS and the probability density vanishes. A general trend is manifest: the ABS is more localized near the boundary when the dispersion dives away from the continuum into the midgap regime. Let us concentrate on the peaks (indicated by the blue and pink arrows) near the open boundary first. It is rather interesting that the most pronounced feature in the probability density profile (blue arrow) occurs at the dip of the dispersion. In fact, by integrating over all momenta, it is easy to check that the peaks in the SDOS come from the dips in the dispersion. The other peak (pink arrow) in the probability density profile arises due to the Van Hove singularity. Note that the blue dashed line corresponds to the transverse momentum where the hole packet (near the Γ point) disappears and the electron pocket (near the X point) is almost empty as well. Thus, the density of states is greatly enhanced and leads to the peak structure in the probability density. However, since its energy lies inside the continuum, the peak structure (pink arrow) is unlikely to remain sharp in realistic situations.

In addition to the peak features, it is also interesting to explore the quantum interference patterns in the momentum-resolved probability density. Close to the blue dashed line, stripe oscillations appear and extend into the bulk regime. The enhanced interference pattern comes from the fact that the solutions for z_i are almost real, making the oscillation period longer and visible. On the other hand, near the $k_y=0$ regime, the solutions for z_i are complex. Linear combinations of the four solutions cancel out the quantum interferences and make the probability density profile more or less smooth.

In FT-STS, one looks for magic spots after Fourier transforming the spectroscopy data. These magic spots arise from enhanced quasiparticle interferences between pronounced peaks in the SDOS. Gradually scanning the energy from zero, we hit the first peak in SDOS as shown in Fig. 2. The dominant quasiparticle scattering comes from q_1 and leads to enhanced interferences at the transfer momentum $Q_1 = \pm 2q_1 \simeq \pm 0.38\pi$. As we further increase the energy, the second peak in the local density of states reigns. The quasiparticle scattering should lead to another magic spot at the transfer momentum $Q_2 = \pm 2q_2 \simeq \pm 1.44\pi$. However, since there exist other ABSs at this energy, we expect that the magic spots at Q_2 are likely to be weaker than those at Q_1.

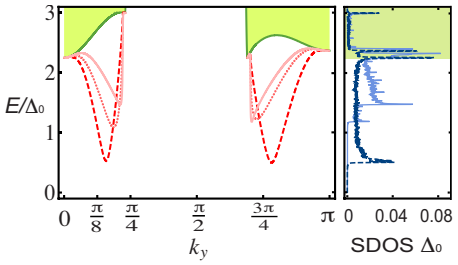

FIG. 3. (Color online) The dispersions of ABS with different surface potentials $V_0/|t_1|=0.08$, 0.16, and 0.40 are showed as solid, dotted, and dashed lines, respectively. On the right-hand side, the surface density of states with $V_0/|t_1|=0.08$ and 0.40 are plotted as light solid and dark dashed lines for comparison.

The ABS in the superconducting iron pnictides occurs at finite energy and thus depends on microscopic details. It is important to explore how the above predictions change when the boundary potential V_0 varies. We show the ABS dispersions with several reasonable choices for the boundary potential V_0 in Fig. 3. The detailed shape of the dispersion is sensitive to the boundary potential. As the boundary potential V_0 increases, the dispersion dives further into the midgap regime. However, several generic features remain robust: the spectral weight transfer inside the midgap regime is significant and there exists a sharp peak in the SDOS. Therefore, the predictions in previous paragraphs remain qualitatively correct but may suffer some quantitative corrections.

In summary, we study the ABS in iron pnictide superconductors, including both the lattice effects and the boundary potential carefully. It is rather surprising that significant spectral weights in the midgap regime emerge, leading to easy detection in realistic experiments. Furthermore, we analyze the locations of these magic spots from quasiparticle interferences and propose a direct experimental verification by the Fourier-transformed scanning tunneling spectroscopy. In recent theoretical investigations, interorbital and interband pairings in iron pnictides are also discussed and studied.[41,42] In principle, the method we developed here can be applied to solve for the ABS in the presence of the interorbital or interband pairing but the detailed analysis remains open and requires further investigations.

We thank G.-Y. Guo for fruitful discussions and acknowledge support from the National Science Council in Taiwan through Grant No. NSC-97-2112-M-007-022-MY3 and partial financial support from the National Center for Theoretical Sciences in Taiwan.

[1] Y. Kamihara, T. Watanabe, M. Hirano, and H. Hosono, J. Am. Chem. Soc. **130**, 3296 (2008).

[2] M. Rotter, M. Tegel, and D. Johrendt, Phys. Rev. Lett. **101**, 107006 (2008).

[3] J. H. Tapp, Z. Tang, B. Lv, K. Sasmal, B. Lorenz, P. C. W. Chu, and A. M. Guloy, Phys. Rev. B **78**, 060505(R) (2008).

[4] F.-C. Hsu, J.-Y. Luo, K.-W. Yeh, T.-K. Chen, T.-W. Huang, P. M. Wu, Y.-C. Lee, Y.-L. Huang, Y.-Y. Chu, D.-C. Yan, and M.-K.

Wu, Proc. Natl. Acad. Sci. U.S.A. **105**, 14262 (2008).
[5] M. R. Norman, Physics **1**, 21 (2008), and references in this introducing paper.
[6] K. Ishida, Y. Nakai, and H. Hosono, J. Phys. Soc. Jpn. **78**, 062001 (2009).
[7] H.-J. Grafe, D. Paar, G. Lang, N. J. Curro, G. Behr, J. Werner, J. Hamann-Borrero, C. Hess, N. Leps, R. Klingeler, and B. Büchner, Phys. Rev. Lett. **101**, 047003 (2008).
[8] Y. Nakai, K. Ishida, Y. Kamihara, M. Hirano, and H. Hosono, J. Phys. Soc. Jpn. **77**, 073701 (2008).
[9] K. Matano, Z. A. Ren, X. L. Dong, L. L. Sun, Z. X. Zhao, and G. Q. Zheng, EPL **83**, 57001 (2008).
[10] H. Luetkens, H.-H. Klauss, R. Khasanov, A. Amato, R. Klingeler, I. Hellmann, N. Leps, A. Kondrat, C. Hess, A. Kohler, G. Behr, J. Werner, and B. Büchner, Phys. Rev. Lett. **101**, 097009 (2008).
[11] J. D. Fletcher, A. Serafin, L. Malone, J. G. Analytis, J.-H. Chu, A. S. Erickson, I. R. Fisher, and A. Carrington, Phys. Rev. Lett. **102**, 147001 (2009).
[12] C. W. Hicks, T. M. Lippman, M. E. Huber, J. G. Analytis, J.-H. Chu, A. S. Erickson, I. R. Fisher, and K. A. Moler, Phys. Rev. Lett. **103**, 127003 (2009).
[13] R. T. Gordon, N. Ni, C. Martin, M. A. Tanatar, M. D. Vannette, H. Kim, G. D. Samolyuk, J. Schmalian, S. Nandi, A. Kreyssig, A. I. Goldman, J. Q. Yan, S. L. Bud'ko, P. C. Canfield, and R. Prozorov, Phys. Rev. Lett. **102**, 127004 (2009).
[14] N. Terasaki, H. Mukuda, M. Yashima, Y. Kitaoka, K. Miyazawa, P. M. Shirage, H. Kito, H. Eisaki, and A. Iyo, J. Phys. Soc. Jpn. **78**, 013701 (2009).
[15] K. Hashimoto, T. Shibauchi, T. Kato, K. Ikada, R. Okazaki, H. Shishido, M. Ishikado, H. Kito, A. Iyo, H. Eisaki, S. Shamoto, and Y. Matsuda, Phys. Rev. Lett. **102**, 017002 (2009).
[16] L. Malone, J. D. Fletcher, A. Serafin, A. Carrington, N. D. Zhigadlo, Z. Bukowski, S. Katrych, and J. Karpinski, Phys. Rev. B **79**, 140501(R) (2009).
[17] X. G. Luo, M. A. Tanatar, J.-Ph. Reid, H. Shakeripour, N. Doiron-Leyraud, N. Ni, S. L. Bud'ko, P. C. Canfield, Huiqian Luo, Z. Wang, H.-H. Wen, R. Prozorov, and L. Taillefer, Phys. Rev. B **80**, 140503(R) (2009).
[18] L. Zhao, H. Y. Liu, W. T. Zhang, J. Q. Meng, X. W. Jia, G. D. Liu, X. L. Dong, G. F. Chen, J. L. Luo, N. L. Wang, W. Lu, G. L. Wang, Y. Zhou, Y. Zhu, X. Y. Wang, Z. X. Zhao, Z. Y. Xu, C. T. Chen, and X. J. Zhou, Chin. Phys. Lett. **25**, 4402 (2008).
[19] H. Ding, P. Richard, K. Nakayama, K. Sugawara, T. Arakane, Y. Sekiba, A. Takayama, S. Souma, T. Sato, T. Takahashi, Z. Wang, X. Dai, Z. Fang, G. F. Chen, J. L. Luo, and N. L. Wang, EPL **83**, 47001 (2008).
[20] T. Kondo, A. F. Santander-Syro, O. Copie, C. Liu, M. E. Tillman, E. D. Mun, J. Schmalian, S. L. Bud'ko, M. A. Tanatar, P. C. Canfield, and A. Kaminski, Phys. Rev. Lett. **101**, 147003 (2008).
[21] K. Terashima, Y. Sekiba, J. H. Bowen, K. Nakayama, T. Kawahara, T. Sato, P. Richard, Y.-M. Xu, L. J. Li, G. H. Cao, Z.-A. Xu, H. Ding, and T. Takahashi, Proc. Natl. Acad. Sci. U.S.A. **106**, 7330 (2009).
[22] D. J. Singh and M. H. Du, Phys. Rev. Lett. **100**, 237003 (2008).
[23] K. Kuroki, S. Onari, R. Arita, H. Usui, Y. Tanaka, H. Kontani, and H. Aoki, Phys. Rev. Lett. **101**, 087004 (2008).
[24] I. I. Mazin, D. J. Singh, M. D. Johannes, and M. H. Du, Phys. Rev. Lett. **101**, 057003 (2008).
[25] A. V. Chubukov, D. V. Efremov, and I. Eremin, Phys. Rev. B **78**, 134512 (2008).
[26] F. Wang, H. Zhai, Y. Ran, A. Vishwanath, and D.-H. Lee, Phys. Rev. Lett. **102**, 047005 (2009).
[27] C. Platt, C. Honerkamp, and W. Hanke, New J. Phys. **11**, 055058 (2009).
[28] D. Wang, Y. Wan, and Q.-H. Wang, Phys. Rev. Lett. **102**, 197004 (2009).
[29] S. Onari and Y. Tanaka, Phys. Rev. B **79**, 174526 (2009).
[30] M. A. N. Araújo and P. D. Sacramento, Phys. Rev. B **79**, 174529 (2009).
[31] A. A. Golubov, A. Brinkman, Yukio Tanaka, I. I. Mazin, and O. V. Dolgov, Phys. Rev. Lett. **103**, 077003 (2009).
[32] D. Zhang, Phys. Rev. Lett. **103**, 186402 (2009).
[33] P. Ghaemi, F. Wang, and A. Vishwanath, Phys. Rev. Lett. **102**, 157002 (2009).
[34] C. R. Hu, Phys. Rev. Lett. **72**, 1526 (1994).
[35] J. E. Hoffman, K. McElroy, D.-H. Lee, K. M. Lang, H. Eisaki, S. Uchida, and J. C. Davis, Science **297**, 1148 (2002).
[36] K. McElroy, R. W. Simmonds, J. E. Hoffman, D.-H. Lee, J. Orenstein, H. Eisaki, S. Uchida, and J. C. Davis, Nature (London) **422**, 592 (2003).
[37] S. Raghu, X.-L. Qi, C.-X. Liu, D. J. Scalapino, and S.-C. Zhang, Phys. Rev. B **77**, 220503(R) (2008).
[38] Y. Ran, F. Wang, H. Zhai, A. Vishwanath, and D.-H. Lee, Phys. Rev. B **79**, 014505 (2009).
[39] T. Pereg-Barnea and H.-H. Lin, EPL **69**, 791 (2005).
[40] W.-M. Huang and H.-H. Lin, Phys. Rev. B **78**, 224522 (2008).
[41] A. Moreo, M. Daghofer, A. Nicholson, and E. Dagotto, Phys. Rev. B **80**, 104507 (2009).
[42] A. V. Chubukov, M. G. Vavilov, and A. B. Vorontsov, Phys. Rev. B **80**, 140515(R) (2009).